He, B., *et al.*: Numerical Investigation of Molten Salt-Based Nanofluid Laminar ...
THERMAL SCIENCE: Year 2021, Vol. 25, No. 5A, pp. 3427-3439

3427

NUMERICAL INVESTIGATION OF MOLTEN SALT-BASED NANOFLUID LAMINAR HEAT TRANSFER IN A CIRCULAR TUBE USING EULERIAN-LAGRANGIAN METHOD

by

Boshu HE[a,b] and Zhaoping YING[a*]

[a] Institute of Combustion and Thermal Systems,
School of Mechanical, Electronic and Control Engineering,
Beijing Jiaotong University, Beijing, China
[b] School of Mechanical and Power Engineering,
Cangzhou Jiaotong College, Huanghua, China

Molten salt-based nanofluid in a laminar region of a circular tube with constant wall heat flux was numerically investigated. An Eulerian-Lagrangian method, discrete phase model, was used to predict the heat transfer performance of nanofluid, considering the factors of inlet Reynolds number, the mass concentration of the nanoparticles, and nanoparticles diameter. Validation results were found in a good match with experimental results obtained from the literature. Numerical results showed that the heat transfer performance of nanofluid was considerably better than that of pure molten salt. The local heat transfer coefficient and Nusselt number of nanofluid are about 30% higher than these of pure molten salt and increase with an increase of Reynolds number and nanoparticles concentration. Moreover, the heat transfer performance of nanofluid with the small size of the nanoparticles (10~100 nm) is improved significantly.

Key words*: molten salt-based nanofluid, laminar, Eulerian-Lagrangian method, heat transfer, Numerical simulation*

Introduction

Solar energy is gradually widely used as a kind of sustainable energy source in concentrating solar power (CSP) systems, which is one of the most promising power generation technologies in the future. For CSP systems, molten salt is a kind of suitable working fluid for its high heat capacity [1].

Some studies had been conducted on the characteristics of flow and heat transfer of molten salt. Xiao *et al.* [2] found the frictional pressure drop of molten salt HITEC (53% KNO_3/40% $NaNO_2$/7% $NaNO_3$, mass concentration) agreed well with the theoretical prediction within 15% in laminar and turbulent flow regions. Wu *et al.* [3] prepared a new molten salt and found a good agreement between their experimental data and the predictions of Sieder-Tate correlation [4]. However, Kunugi *et al.* [5] revealed that the poor heat transfer performance of molten salt resulted in laminarization phenomena and non-uniform heating.

Choi and Eastman [6] found the thermal performance improvement of *nanofluid* with a dramatic increase of thermal conductivity when they added nanoparticles into the basic fluid.

---

* Corresponding author, e-mail: zhaoping@bjtu.edu.cn

After then more research had been reported that the better thermal performance of nanofluid comparatively with base fluid [7, 8], which could promote thermal applications like heat exchangers [9] and electronics cooling [10]. Moreover, the heat transfer enhancement of nanofluid had been studied extensively on the solar thermal system. Sokhansefat *et al.* [11] studied the Al_2O_3-synthetic oil nanofluid in a parabolic trough collector tube. They found its heat transfer coefficient increased with the increase of nanoparticles concentrations. Menbari *et al.* [12] studied the CuO-water nanofluid in the direct absorption solar collector. They revealed that the thermal efficiency of the collector increased as increasing the volume fraction and flow rate of the nanofluid. Ghaderian *et al.* [13] found that the CuO-water nanofluid with a volume fraction of 0.03% improved the efficiency of the evacuated tube solar collector by 14% comparatively with pure water.

Some studies [14-17] revealed the better thermal performance of molten salt-based nanofluid. Zhang *et al.* [14] prepared Al_2O_3-Li_2CO_3/Na_2CO_3/K_2CO_3 nanofluid using a two-step aqueous method. Their measurement data showed that the molten salt suspended with Al_2O_3 nanoparticles had higher specific heat capacity and thermal conductivity comparatively with pure molten salt. Hu *et al.* [15, 16] prepared the Al_2O_3- and SiO_2-solar salt nanofluid and found 2.0% (mass fraction) Al_2O_3-solar salt nanofluid or 1.0% (mass fraction) SiO_2-solar salt nanofluid achieved the maximum enhancement of specific heat capacity by 8.3% or 26.8%, respectively. Ho and Pan [17] investigated the optimum concentration of Al_2O_3 nanoparticles to maximize the specific heat capacity of HITEC. Their results showed that the Al_2O_3-HITEC nanofluid with a mass fraction of 0.063% maximally enhanced the specific heat capacity by 19.9% comparatively with pure HITEC.

However, there is a gap in the literature in the area of heat transfer of molten salt-based nanofluid. Only Ho and Pan [18] conducted an experiment to research the heat transfer performance of HITEC-based nanofluid-flowing in a circular tube. But, they merely considered the impact of nanoparticles concentration on the heat transfer enhancement. Therefore, in this paper, alumina molten salt-based nanofluid is numerically investigated, considering the factors of entrance Reynolds number, the mass concentration of nanoparticles, and nanoparticles diameter on nanofluid's laminar convective heat transfer performance in a circular tube. The discrete phase model (DPM) based on the Eulerian-Lagrangian frame [19, 20] was employed. This paper might work as a supplement to the field of heat transfer performance of molten salt-based nanofluid.

Numerical simulations

A simplified 2-D axisymmetric model is used based on the experiments by Ho and Pan [18]. As shown in fig. 1, a horizontal tube receives constant wall heat flux with a diameter of 0.0021 m and a length of 0.12 m. Different entrance Reynolds numbers (68, 268), different nanoparticles diameters (10 nm, 20 nm, 40 nm, 75 nm, and 100 nm), and different mass concentrations (0.016 wt.%, 0.063 wt.%, 0.125 wt.%, and 0.25 wt.%) are considered.
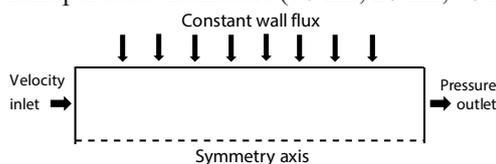
The thermophysical properties for the alumina nanoparticles [1], stainless steel tube [14], and HITEC [21] are given in tab. 1. It is important to note that the temperature used here is in Kelvin.

Figure 1. Schematic of the 2-D axissymmetric geometry

He, B., *et al.*: Numerical Investigation of Molten Salt-Based Nanofluid Laminar ...
THERMAL SCIENCE: Year 2021, Vol. 25, No. 5A, pp. 3427-3439

3429

Table 1. Thermophysical properties of the nanoparticles and tube

Properties	Al_2O_3 [1]	Stainless steel [14]	HITEC [21]
ρ [kg^{-3}]	3880	7900	$-0.733T + 2280.21895$
c_p [Jkg^{-1}K^{-1}]	733	477	$-T + 1833.15$
k [Wm^{-1}K^{-1}]	36	14.9	$1.6 \cdot 10^{-6}T^2 - 1.25 \cdot 10^{-3}T + 0.78$
μ [Pa·s]	–	–	$\dfrac{\exp(b) + \exp(-b)}{\exp(b) - \exp(-b)} - 0.999, \ b = \dfrac{5.9(T - 9.638)}{990.362}$

Mathematical modelling

The DPM is an Eulerian-Lagrangian approach and able to describe the flow and heat transfer process of two-phase fluid such as Al_2O_3-HITEC nanofluid. In this model, the Lagrangian frame expresses the particles' position, while the Eulerian frame specifies the condition of the continuum through solving the Navier-Stokes equations. Governing equations of continuity, momentum, and energy are given [22]:

– Mass equation

$$\nabla \cdot \left(\rho \vec{V} \right) = 0 \tag{1}$$

– Momentum equation

$$\nabla \cdot \left(\rho \vec{V} \ \vec{V} \right) = -\nabla p + \nabla \cdot \left(\mu \nabla \vec{V} \right) + \vec{S}_m \tag{2}$$

– Energy equation

$$\nabla \cdot \left(\rho \vec{V} c_p T \right) = \nabla \cdot \left(k \nabla T \right) + S_e \tag{3}$$

The source terms S_m and S_e represent the amount of momentum and energy exchange between particles and the base fluid (molten salt HITEC), respectively.

For a single particle, the motion equation is simply defined:

$$\dot{m}_p \frac{\mathrm{d}\vec{V}_p}{\mathrm{d}t_p} = \vec{F}_D + \vec{F}_g + \vec{F}_{others} \tag{4}$$

where t_p is the time that the particle moves from one cell to the adjacent one in the Lagrangian reference frame. The first term on the right side of the equation is the drag force, and the Stokes law is valid for low nanoparticles Reynolds number ($Re_p < 1$):

$$Re_p = \frac{\rho_{bf} d_p V_{av}}{\mu_{bf}} \tag{5}$$

In this study, the drag force, $\vec{F}_D$, can be calculated [22]:

$$\vec{F}_D = \frac{3\mu_{bf} C_d Re_p}{4 d_p^2 \rho_p} \dot{m}_p \left(\vec{V}_{bf} - \vec{V}_p \right) \tag{6}$$

where C_d is drag force coefficient. The second term on the right side of the eq. (4) is the gravity:

$$\vec{F}_g = \dot{m}_p \frac{\vec{g}(\rho_p - \rho_{bf})}{\rho_p} \tag{7}$$

The third term on the right side of the eq. (4) is $\vec{F}_{\text{others}}$, which includes thermophoretic force, Brownian force, Saffman lift force, *etc*. The Saffman lift force or the force due to shear is calculated [23]:

$$\vec{F}_s = \dot{m}_p \frac{5.2 \nu^{1/2} \rho \delta_{ij}}{\rho_p d_p (\delta_{IK} \delta_{KI})^{1/4}} \left(\vec{V}_f - \vec{V}_p \right) \tag{8}$$

where δ_{ij} is the deformation tensor.

The equation of thermophoretic force $\vec{F}_T$ for particles in a liquid is given by McNab [19]:

$$\vec{F}_T = -D_{T,p} \frac{\nabla T}{T} \tag{9}$$

where $D_{T,p}$ is the coefficient of the thermophoretic force [24].

The components of the Brownian force are modeled as a Gaussian white noise process with spectral intensity $S_{n,ij}$ given by [19]:

$$S_{n,ij} = S_0 \epsilon_{ij} \tag{10}$$

where ϵ_{ij} is the Kronecker delta function, and S_0 is:

$$S_0 = \frac{216 \nu K_B T}{\pi^2 \rho_{bf} d_p^5 \left(\dfrac{\rho_p}{\rho_{bf}} \right)^2 C_c} \tag{11}$$

where K_B is the Boltzmann constant ($1.3807 \cdot 10^{-23}$ J/K).

Amplitudes of the Brownian force components [24]:

$$F_{B_i} = \dot{m}_p \xi_i \left(\frac{\pi S_0}{\Delta t} \right)^{1/2} \tag{12}$$

where ξ_i are zero-mean, unit-variance-independent Gaussian random numbers.

The contribution of forced due to virtual mass, $\vec{F}_V$:

$$\vec{F}_v = 0.5 \dot{m}_p \frac{\rho_{bf}}{\rho_P} \left(\vec{V}_p \nabla \vec{V} - \frac{d\vec{V}_p}{dt} \right) \tag{13}$$

The contribution of force generated due to the pressure gradient, $\vec{F}_p$, in the fluid:

$$\vec{F}_p = \dot{m}_p \frac{\rho_{bf}}{\rho_P} \vec{V}_p \nabla \vec{V} \tag{14}$$

The amount of heat transfer exchange for each particle is calculated from energy balance, which will be implemented as an energy source term in eq. (3):

$$Q_s = \dot{m}_p c_{p,p} \left(T_{p,in} - T_{p,out} \right) \tag{15}$$

Particles flow rate $\dot{m}_p$ in each cell will be conserved as there is no mass exchange. The $c_{p,p}$ is particle specific heat, $T_{p,in}$ and $T_{p,out}$ are particle temperature at the inlet and outlet of a cell, respectively. To find $T_{p,in}$ and $T_{p,out}$, the exchanged heat at the surface of a particle:

$$\dot{m}_p c_{p,p} \frac{dT_p}{dt} = h A_p \left(T_c - T_p \right) \tag{16}$$

For a spherical particle, the heat transfer coefficient can be solved from the correlation [25]:

$$\frac{h d_p}{k_p} = 2 + 0.6 \mathrm{Re}_p^{0.5} \mathrm{Pr}^{1/3} \tag{17}$$

Boundary conditions

As shown in fig. 1, the axisymmetric 2-D tube is adopted in this study. The nanofluid enters the tube at a uniform temperature 573 K. Inlet velocity is set based on entrance Reynolds number, while zero pressure is specified for the outlet. In the wall of the test tube, no-slip boundary condition and constant heat flux are considered. For boundary conditions of nanoparticles in the DPM model, the homogeneous injection from the inlet is set, and the *Escape*, *Escape,* and *Reflect* are chosen for inlet, outlet, and wall, respectively [26].

Discretization method and validation

The commercial software ANSYS FLUENT 18.0 [24] is used to solve governing equations. The SIMPLE algorithm is used for the pressure/velocity coupling. The second-order upwind scheme is used for the convective and diffusive terms. The scaled residuals for the continuity, two velocity components, and energy are all set as 10^{-7}. Suitable under relaxation factors are adopted to solve the equations smoothly. Iterations are first carried out, regarding the base fluid as a single-phase fluid. Later, the DPM is enabled after the computation of base fluid achieves convergence.

The model validation process includes grid independency test and code accuracy check. Simulations are carried out initially on pure HITEC to test the grid independency. Different mesh sizes (5×500, 10×1000, 20×2000, 30×3000, 40×4000, 50×5000, 100×2000, and 100×4000) are considered. Figure 2 shows the obtained numerical results, in which the local Nusselt numbers are seen as a function of non-dimensional distance and they are compared in different meshes at Re = 68. The non--dimensional distance, x^*, is defined as $x^* = x/\mathrm{PrRe}D$, and the Prandtl number is defined as $\mathrm{Pr} = c_p \mu / k$. The thermal properties are tem-

Figure 2. Grid independency of the numerical code

perature dependent and are calculated based on the average temperature of the fluid. According to the results, other meshes except 5×500 and 10×1000 indicate grid independency of the code. However, a mesh size of 40×4000 elements is finally chosen to ensure grid independency and meet calculation cost because finer grids are required to injecting nanoparticles into the base fluid in the DPM model [27].
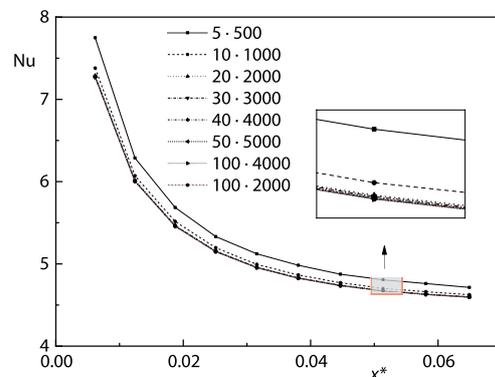
To verify the accuracy of the developed code, simulation of pure HITEC flow in the test section at Re = 68 is conducted. Numerical results of mean Nusselt number are compared with the predictions of conventional Shah-London correlation [28] which is presented in eq. (18). Moreover, to confirm the code accuracy in simulation of nanofluid, the comparisons of local Nusselt number of Al₂O₃-HITEC nanofluid are done among the numerical results, the experimental results of Ho and Pan [18], and the values of fitted correlation:

$$
\text{Nu}_m = \begin{cases} 1.953 \left(x_L^* \right)^{-1/3}, & x_L^* \le 0.03 \\ 4.364 + \dfrac{0.0722}{x_L^*}, & x_L^* > 0.03 \end{cases} \tag{18}
$$

where x_L^* is defined as a non-dimensional length of the test section:

$$
x_L^* = \frac{L}{\text{PrRe}D} \tag{19}
$$

The local heat transfer coefficient, h_x, is calculated:

$$
h_x = \frac{q''}{T_w - T_{m(x)}} \tag{20}
$$

where the heat flux, q'', applied to the fluid can be obtained from the measurement of inlet and outlet temperature of the fluid, based on the energy balance for a constant heat flux tube:

$$
q'' = \frac{\dot{m} c_p \left(T_{out} - T_{in} \right)}{\pi D L} \tag{21}
$$

where $\dot{m}$, c_p, D, and L are the mass-flow rate, specific heat capacity, inner diameter, and length of the test tube, respectively.

Local Nusselt number, Nu_x, is defined:

$$
\text{Nu}_x = \frac{h_x D}{k_f} \tag{22}
$$

where k_f is the thermal conductivity of the HITEC.

The mean fluid temperature is evaluated based on the energy balance and can be shown:

$$
T_{m(x)} = T_{in} + \frac{q'' \pi D x}{\dot{m} c_p} \tag{23}
$$

where the specific heat capacity, c_p, of the Al$_2$O$_3$-HITEC nanofluid with different nanoparticles concentrations is calculated based on the data reported by Ho and Pan [17]. The average heat transfer coefficient is calculated:
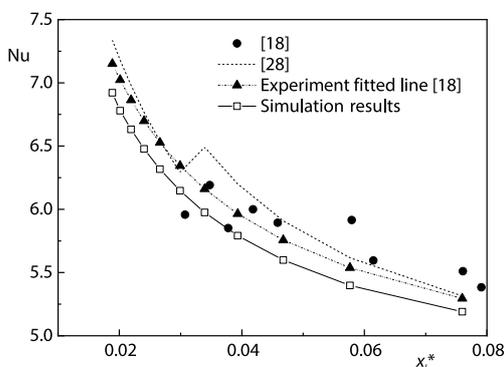
$$
\bar{h} = \frac{q''}{T_w - T_b} \tag{24}
$$

where T_w and T_b are the wall temperature and the average temperature of the inlet and outlet temperature, respectively. Therefore, the mean Nusselt number can be calculated:

$$
\text{Nu}_m = \frac{\bar{h} D}{k_f} \tag{25}
$$

Figure 3 shows that the data of simulation agree well with the predictions of the correlation within 10% and match well with experiment results within ±10%. Such a reasonable agreement in the mean Nusselt number of molten HITEC flow indicates that the present model can be used for the simulation

Figure 3. Validation of the simulation with results of [18] and [28] correlation

He, B., *et al.*: Numerical Investigation of Molten Salt-Based Nanofluid Laminar ...
THERMAL SCIENCE: Year 2021, Vol. 25, No. 5A, pp. 3427-3439

3433

of HITEC doped with alumina nanoparticles. Then the correct model is employed to research alumina-HITEC nanofluid heat transfer performance.

The following figs. 4(a)-4(d) show the DPM simulation accuracy of different mass concentrations of Al$_2$O$_3$-HITEC nanofluid with 0.016 wt.%, 0.063 wt.%, 0.125 wt.%, and 0.25 wt.%. Compared with the results from the experiment and the fitted line, the simulation qualitatively captures the experimental observations' main feature. Quantitatively, fairly good agreement between experimental results and the simulation has been achieved for $x^* \sim 0.025$ at Re = 68. However, for small x^* values, the simulation results deviate from the line fitted from experimental data. Considering the error of fitting line from experimental data scatters, in the error range up to 20%, the simulation confirms good agreement with the experiment.
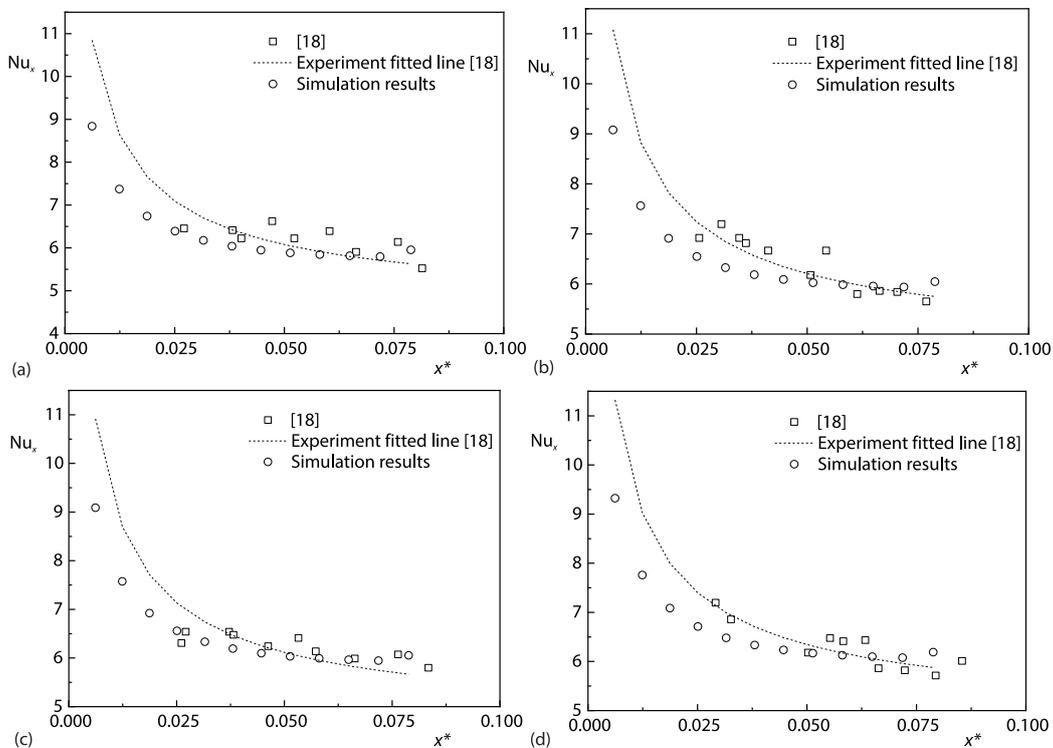

Figure 4. Accuracy of the simulation of Al$_2$O$_3$-HITEC nanofluid with different mass concentrations; (a) 0.016 wt.%, (b) 0.063 wt.%, (c) 0.125 wt.%, (d) 0.25 wt.%

Results and discussions

The validated numerical model is used to investigate the influences of different Reynolds number (68 and 268), different nanoparticles concentrations (0 wt.%, 0.016 wt.%, 0.063 wt.%, 0.125 wt.%, and 0.25 wt.%), and different sizes of nanoparticles (40 nm and 100 nm) on the heat transfer performance of Al$_2$O$_3$-HITEC nanofluid. Numerical results are presented in this section.

Local heat transfer coefficient

The local heat transfer coefficient is calculated by using the eqs. (20) and (21). Figures 5(a) and 5(b) show the local heat transfer coefficient of HITEC with or without Al$_2$O$_3$ nanopar-

ticles along the axial distance (x/D is used for different Reynolds number, because x^* is not suitable for comparison) at Re = 68 and 268, respectively. It is indicated in figs. 5(a) and 5(b) that the heat transfer coefficient increases with the increase of concentration. It is mainly because that the thermophysical properties of HITEC with or without nanoparticles are temperature-dependent, making its Prandtl number and corresponding boundary-layer change along the axial direction of the tube, resulting in an increase of the relative heat transfer coefficient of nanofluid. Besides, the convective heat transfer coefficient decreases as the axial direction distance increases, due to an increase in the temperature difference between the wall and bulk with constant wall heat flux. Also, the comparison between figs. 5(a) and 5(b) shows that the heat transfer coefficient increases with Reynolds number increasing since the larger flow velocity enhances the convective heat transfer.
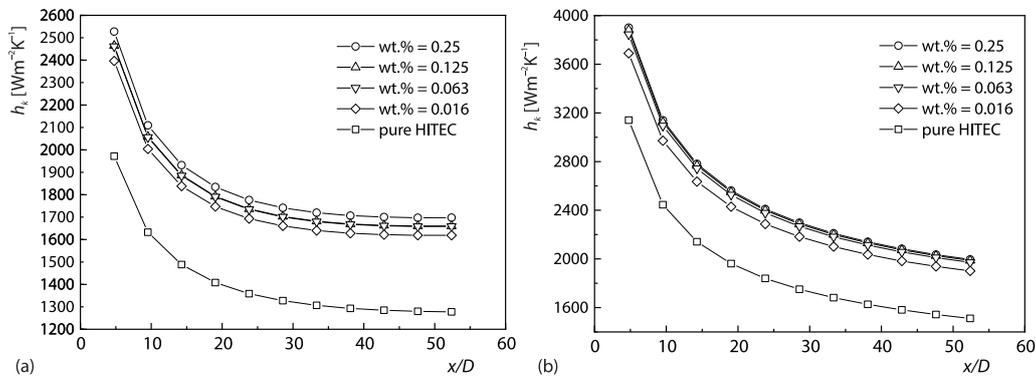

Figure 5. Heat transfer coefficient of Al$_2$O$_3$-HITEC nanofluid with different mass concentrations along axial direction at (a) Re = 68 and (b) Re = 268

The relative heat transfer coefficient ($\eta = h_{x,\text{nf}}/h_{x,\text{bf}}$) is presented in figs. 6(a) and 6(b) at Re = 68 and Re = 268, respectively. It can be seen from two figures that the heat transfer coefficient is enhanced by adding nanoparticles into pure HITEC and increases as increasing the mass concentration. In the case of 0.25 wt.% nanofluid which shows the largest heat transfer enhancement, the improvement percentage is more than 29% or 28% at the entrance region and increases to about 33% or 32% at the channel exit, respectively, when Re = 68 or Re = 268. Besides, the heat transfer enhancements for 0.063 wt.% and 0.125 wt.% are nearly the same,
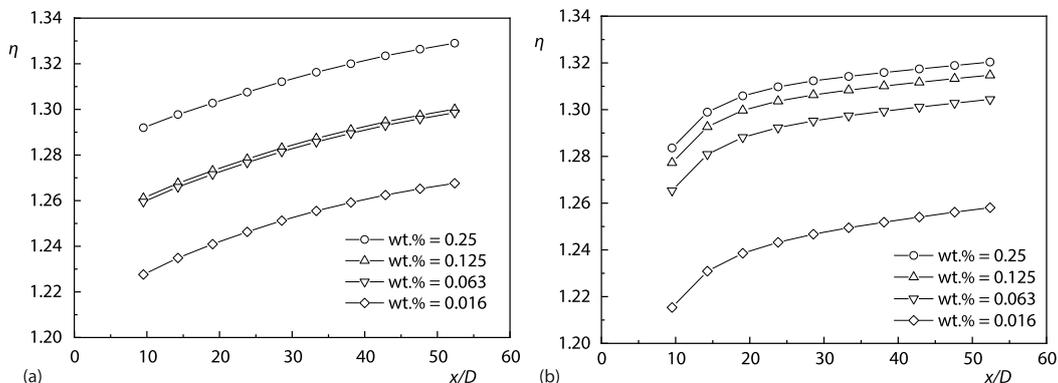

Figure 6. Relative heat transfer coefficient of different mass concentrations of Al$_2$O$_3$-HITEC nanofluid along axial direction at (a) Re = 68 and (b) Re = 268

He, B., *et al.*: Numerical Investigation of Molten Salt-Based Nanofluid Laminar ...
THERMAL SCIENCE: Year 2021, Vol. 25, No. 5A, pp. 3427-3439

3435

which fits well with the experimental results reported by Ho and Pan [18]. Also, the relative heat transfer coefficient of Al_2O_3-HITEC nanofluid with various concentrations increases with axial location, and this trend is more noticeable for nanofluid with larger concentration because the thermal conductivity is a function of the nanoparticles volume fraction. By comparing these two figures, the relative heat transfer coefficient is found only a little change, as the flow is in the laminar region.

The following figs. 7(a)-7(d) give an axial profile of the local heat transfer coefficient of Al_2O_3-HITEC nanofluid with different mass concentrations and different sizes of nanoparticles at Re = 68. On the one hand, it is indicated in these figures that for all four mass concentrations, the nanofluid with small nanoparticles has a stronger ability to improve heat transfer, showing that the addition of nanoparticles with different sizes and fractions is beneficial to enhance the heat transfer performance of pure HITEC. On the other hand, for nanofluid with small mass concentration like 0.016 wt%, its heat transfer coefficient increases as the size of the nanoparticles decreases. The possible reasons can be explained that with the reduction in particle size, uniform distribution along the channel radial direction and effective particle surface area enhance the heat transfer coefficient of nanofluid. While as the mass concentration rises, the nanofluid with all size nanoparticles shows considerable heat transfer enhancement comparatively with pure HITEC, but the difference of heat transfer performance between different nanoparticles size becomes not obvious. It might because the nanoparticles concentration is the primary influencing factor on the heat transfer performance of nanofluid, compared with nanoparticles size.
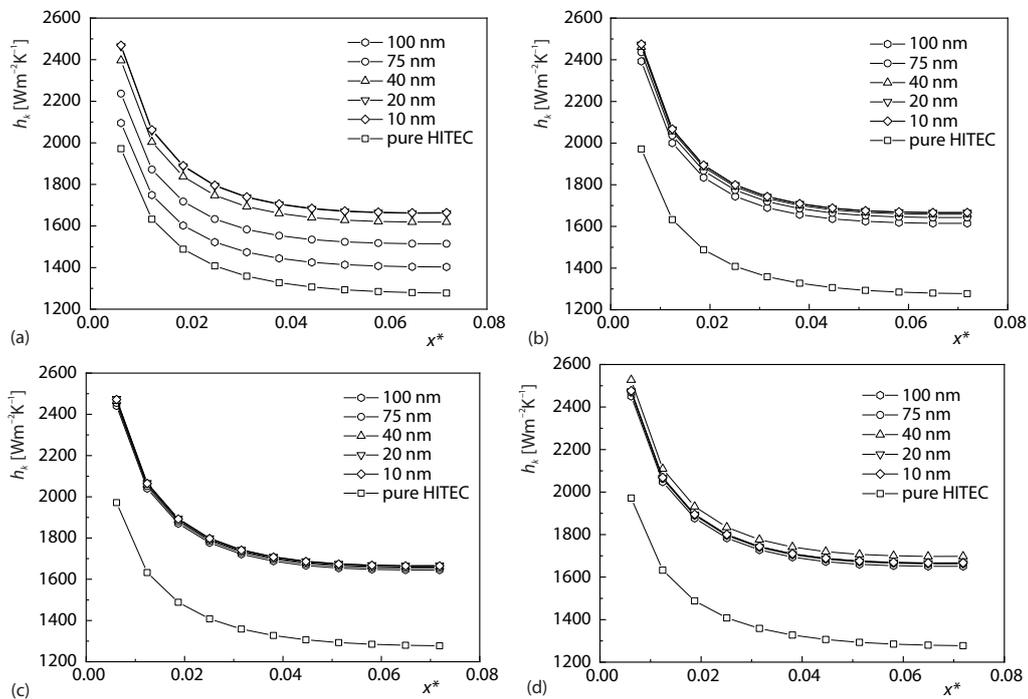

Figure 7. Heat transfer coefficient of Al_2O_3-HITEC nanofluid with different nanoparticles diameters along axial direction with (a) 0.016 wt.%, (b) 0.063 wt.%, (c) 0.125 wt.%, and (d) 0.25 wt.%

Local Nusselt numbers

The effects of Al_2O_3 nanoparticles concentration on the local Nusselt number at Re = 68 and Re = 268 are shown in figs. 8(a) and 8(b), respectively. In these cases, the diameter of Al_2O_3 nanoparticles is 40 nm. From two figures, it can be found that for various nanoparticles concentrations, the local Nusselt numbers of Al_2O_3-HITEC nanofluid decrease as increasing the axial non-dimensional distance. Besides, the local Nusselt numbers of Al_2O_3-HITEC nanofluid increase with the mass concentration increasing and demonstrate relatively high enhancement (up to 28-33%) compared with the counterparts of pure HITEC. Besides, a comparison between figs. 8(a) and 8(b) shows that the local Nusselt number increases with Reynolds number.
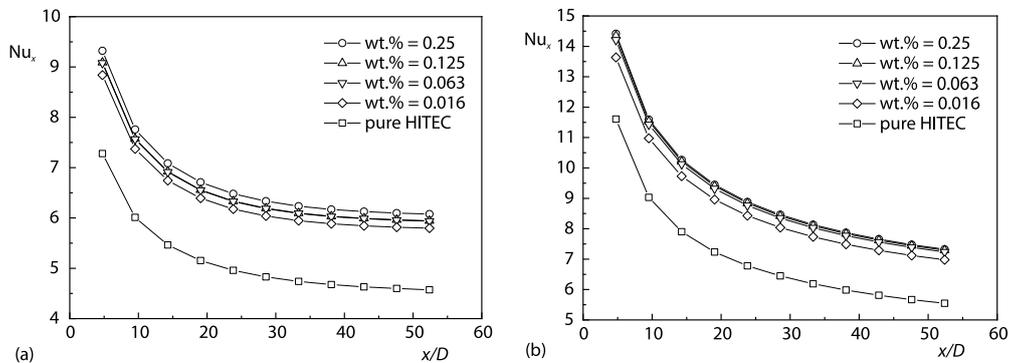

Figure 8. The Nu$_x$ of Al$_2$O$_3$-HITEC nanofluid with different concentrations at (a) Re = 68 and (b) Re = 268

Then, the local Nusselt number along the axial non-dimensional axial distance at Re = 68 is plotted in figs. 9(a)-9(d), for nanofluid with sets of nanoparticles size and mass concentration. It can be seen from figs. 9(a)-9(d) that the local Nusselt number of nanofluid increases with nanoparticles size reducing for all mass concentrations. The highest improvement is observed at a higher mass concentration (like 0.25 wt.%) and a smaller nanoparticles size (like 40 nm). Therefore, there might exist an optimized combination of mass concentration and nanoparticles size for Al_2O_3-HITEC nanofluid.

Conclusion

To explore the heat transfer performance of molten salt-based nanofluid, the laminar convective heat transfer of Al_2O_3-HITEC nanofluid inside a tube is numerically studied by employing the Eulerian-Lagrangian two-phase method. The effects of Reynolds number, nanoparticles concentration, and nanoparticles size on the heat transfer performance of HITEC with or without Al_2O_3 nanoparticles are considered.

The results show that the local heat transfer coefficient and Nusselt number of Al_2O_3-HITEC nanofluid are about 30% higher than these of pure HITEC, which means that heat transfer performance enhancement is achieved by adding Al_2O_3 nanoparticles into molten salt HITEC. Specifically, the heat transfer coefficient and Nusselt number of Al_2O_3-HITEC nanofluid increase with an increase of Reynolds number and nanoparticles concentration. Besides, the heat transfer performance of Al_2O_3-HITEC nanofluid with the small size of the nanoparticles (10~100 nm) is improved significantly.
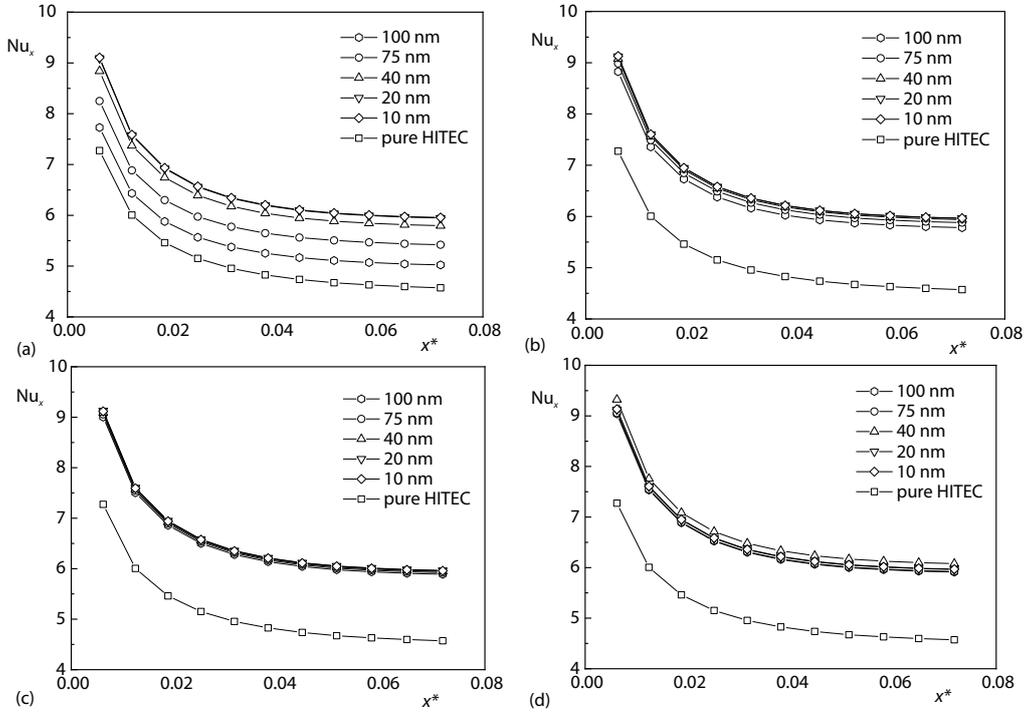
He, B., *et al.*: Numerical Investigation of Molten Salt-Based Nanofluid Laminar ...
THERMAL SCIENCE: Year 2021, Vol. 25, No. 5A, pp. 3427-3439

3437

Figure 9. The Nu_x of Al₂O₃-HITEC nanofluid with different nanoparticles diameters along the axial direction; (a) 0.016 wt%, (b) 0.063 wt%, (c) 0.125 wt%, and (d) 0.25 wt%

Nomenclature

A – area, [m^2]
c – cell
C_d – drag force coefficient
c_p – specific heat capacity, [Jkg^{-1}K^{-1}]
d_p – particle diameter, [m]
D – tube diameter, [m]
$\vec{F}$ – total force acting on the force, [N]
$\vec{F}_D$ – drag force, [N]
F_B – Brownian force, [N]
$\vec{F}_T$ – thermophoretic force, [N]
$\vec{F}_L$ – Saffman's lift force, [N]
F_p – pressure gradient force, [N]
F_V – virtual mass force, [N]
h – heat transfer coefficient, [Wm^{-2}K^{-1}]
L – length, [m]
k – thermal conductivity, [Wm^{-1}K^{-1}]
k_B – Boltzmann constant
$\dot{m}$ – particle flow rate [kgs^{-1}]
Nu – Nusselt number
P – Static pressure, [Nm^{-2}]
Pr – Prandtl number
q'' – heat flux, [Wm^{-2}]
Re – Reynolds number

S_0 – spectral intensity basis
S_e – source term of the energy equation
$\vec{S}_m$ – source term of momentum equation
$S_{n,ij}$ – spectral intensity basis
t – time, [s]
T – temperature, [K]
$\vec{V}$ – velocity of nanofluid, [ms^{-1}]
$\vec{V}_1$ – fluid velocity, [ms^{-1}]
$\vec{V}_p$ – particle velocity, [ms^{-1}]
x – axis distance, [m]
x^* – axis non-dimensional distance
x_L^* – axis non-dimensional length

Greek Letters

δ_{ij} – deformation tensor
μ – dynamic viscosity, [kgm^{-1}s^{-1}]
ρ – density, [kgm^{-3}]

Subscripts

av – average
bf – base fluids
p – particles phase
wt.% – mass fraction

References

[1] Vignarooban, K., *et al.*, Heat Transfer Fluids for Concentrating Solar Power Systems – A Review, *Applied Energy*, *146* (2015), May, pp. 383-396

[2] Xiao, P., *et al.*, Investigations on Heat Transfer Characteristic of Molten salt Flow in Helical Annular Duct, *Applied Thermal Engineering*, *88* (2015), Sept., pp. 22-32

[3] Wu, Y. T., *et al.*, Experimental Study on the Heat Transfer Characteristics of a Low Melting Point Salt in a Parabolic trough Solar Collector System, *Applied Thermal Engineering*, *89* (2015), Oct., pp. 748-754

[4] Holman, J. P., Heat Transfer, 9nd ed., John Wiley and Sons Inc., New York, USA, 2002

[5] Kunugi, T., *et al.*, Direct Numerical Simulation of Turbulent Free-Surface High Prandtl Number Fluid-Flows in Fusion Reactors, *Nuclear Instruments and Methods in Physics Research*, *464* (2001), 1, pp. 165-171

[6] Choi, S. U. S., Eastman, J. A., Enhancing Thermal Conductivity of Fluids with Nanoparticles, *ASME-Publications-Fed*, *231* (1995), 1, pp. 99-106

[7] Bahiraei, M., Heshmatian, S., Graphene Family Nanofluids: A Critical Review and Future Research Directions, *Energy Conversion and Management*, *196* (2019), Sept., pp. 1222-1256

[8] Bahiraei, M., Particle Migration in Nanofluids: A Critical Review, *International Journal of Thermal Sciences*, *109* (2016), Nov., pp. 90-113

[9] Bahiraei, M., *et al.*, Recent Research Contributions Concerning use of Nanofluids in Heat Exchangers: A Critical Review, *Applied Thermal Engineering*, *133* (2018), Mar., pp. 137-159

[10] Bahiraei, M., Heshmatian, S., Electronics Cooling with Nanofluids: A Critical Review, *Energy Conversion and Management*, *172* (2018), Sept. pp. 438-456

[11] Sokhansefat, T., *et al.*, Heat Transfer Enhancement in Parabolic trough Collector Tube Using Al_2O_3/Synthetic Oil Nanofluid, *Renewable and Sustainable Energy Reviews*, *33* (2014), May, pp. 636-644

[12] Menbari, A., *et al.*, Heat Transfer Analysis and the Effect of CuO/Water Nanofluid on Direct Absorption Concentrating Solar Collector, *Applied Thermal Engineering*, *104* (2016), July, pp. 176-183

[13] Ghaderian, J., *et al.*, Performance of Copper Oxide/Distilled Water Nanofluid in Evacuated Tube Solar Collector (ETSC) Water Heater with Internal Coil under Thermosyphon System Circulations, *Applied Thermal Engineering*, *121* (2017), July, pp. 520-536

[14] Zhang, Z., *et al.*, Enhanced Thermal Properties of Li_2CO_3-Na_2CO_3-K_2CO_3 Nanofluids with Nanoalumina for Heat Transfer in High-Temperature CSP Systems, *Journal of Thermal Analysis and Calorimetry*, *128* (2016), 3, pp. 1-10

[15] Hu, Y., *et al.*, Effect of Al_2O_3 Nanoparticle Dispersion on the Specific Heat Capacity of a Eutectic Binary Nitrate Salt for Solar Power Applications, *Energy Conversion and Management*, *142* (2017), June, pp. 366-373

[16] Hu, Y., *et al.*, Forced Convective Heat Transfer Characteristics of Solar Salt-Based SiO_2 Nanofluids in Solar Energy Applications, *Applied Thermal Engineering*, *155* (2019), June, pp. 650-659

[17] Ho, M. X., Pan, C., Optimal Concentration of Alumina Nanoparticles in Molten Hitec Salt to Maximize Its Specific Heat Capacity, *International Journal of Heat and Mass Transfer*, *70* (2014), Mar., pp. 174-184

[18] Ho, M. X., Pan, C., Experimental Investigation of Heat Transfer Performance of Molten HITEC Salt Flow with Alumina Nanoparticles, *International Journal of Heat and Mass Transfer*, *107* (2016), Apr., pp. 1094-1103

[19] Bahiraei, M., A Numerical Study of Heat Transfer Characteristics of CuO-water Nanofluid by Euler-Lagrange Approach, *Journal of Thermal Analysis and Calorimetry*, *123* (2016), 2, pp. 1591-1599

[20] Fard, M. H., *et al.*, Numerical Study of Convective Heat Transfer of Nanofluids in a Circular Tube Two-phase Model *vs*. Single-Phase Model, *International Communications in Heat and Mass Transfer*, *37* (2010), 1, pp. 91-97

[21] Boerema, N., *et al.*, Liquid Sodium *vs*. Hitec as a Heat Transfer Fluid in Solar Thermal Central Receiver Systems, *Solar Energy*, *86* (2012), 9, pp. 2293-2305

[22] Das, S. K., *et al.*, Nanofluids Science and Technology, John Wiley and Sons, Hoboken, N. J., USA, 2008

[23] Saffman, P. G. T., The Lift on a Small Sphere in a Slow Shear Flow, *Journal of Fluid Mechanics*, *22* (2) (1965), 2, pp. 385-400

[24] ***, Manual. FLUENT18.0 User. Fluent Incorporated, 2017

[25] Minkowycz, W. J., *et al.*, Handbook of Numerical Heat Transfer, 2nd ed., John Wiley and Sons, Hoboken, N. J., USA, 2006, p.71

[26] Ying, Z., *et al.*, Comparisons of Single-Phase and Two-Phase Models for Numerical Predictions of Al_2O_3/Water Nanofluids Convective Heat Transfer, *Advanced Powder Technology*, *31* (2020), 7, pp. 3050-3061

He, B., *et al.*: Numerical Investigation of Molten Salt-Based Nanofluid Laminar ...
THERMAL SCIENCE: Year 2021, Vol. 25, No. 5A, pp. 3427-3439

3439

[27] Kumar, N., Puranik, B. P., Numerical Study of Convective Heat Transfer with Nanofluids in Turbulent Flow Using a Lagrangian-Eulerian Approach, *Applied Thermal Engineering*, *111* (2017), Jan., pp. 1674-1681
[28] Shah, R. K., London A. L., Laminar Flow Forced Convection in Ducts, Academic Press, New York, USA, 1978, pp. 124-129